

Lyman-Alpha Absorption Systems and the Nearby Galaxy Distribution

Norman A. Grogin and Margaret J. Geller

Harvard-Smithsonian Center for Astrophysics, 60 Garden Street, Cambridge, MA 02138

E-mail: ngrogin,mgeller@cfa.harvard.edu

ABSTRACT

We study the galaxy number density (smoothed on a $5h^{-1}$ Mpc scale) around 18 low-redshift Lyman-alpha absorbers previously observed with *HST*. The absorbers lie in the foregrounds of Mrk 335, Mrk 421, Mrk 501, I Zw 1, and 3C 273, all within regions where there are now complete redshift surveys to $m_{Zw} = 15.5$. We construct a smoothed galaxy number density field from the redshift survey data and determine the distribution of densities at the Lyman-alpha absorber locations. We also find the distribution of galaxy number density for a variety of test samples: all galaxy locations within the Center for Astrophysics Redshift Survey (CfA2), CfA2 galaxy locations along randomly selected lines of sight, and randomly chosen redshifts along random lines of sight.

The Lyman-alpha absorbers are present in dense regions of the survey, but occur far more frequently in underdense regions than do typical luminous galaxies. The distribution of smoothed galaxy density around the Lyman-alpha absorbers is inconsistent at the 4σ level with the density distribution around survey galaxies. It is highly consistent with a density distribution at randomly chosen redshifts along random lines of sight. This supports earlier evidence that the nearby, low column density ($\log N_{HI} \lesssim 14$) Lyman-alpha forest systems are spatially distributed at random; they are not well correlated with the local large-scale structure.

Subject headings: large-scale structure of the universe — quasars :
absorption lines — intergalactic medium

1. Introduction

The spectra of high-redshift QSOs display a dense network of absorption lines blueward of the QSO Ly α emission, first recognized by Lynds (1971) as low column density Ly α absorption in the rest frame of intervening discrete systems (cf. reviews by Bajtlik 1993; Weymann 1993). With the advent of the *HST*, this

“Ly α forest” could be studied at wavelengths below the atmospheric UV cutoff, corresponding to absorbers with redshift $z \lesssim 1.6$. Because the Ly α forest reveals a considerable population of very tenuous structures ($N_{H\text{I}} > 10^{12} \text{ cm}^{-2}$) across cosmological distances ($z \lesssim 4$), there has been great interest in determining the nature of the absorbers: galactic, intergalactic, or both.

Early studies of the redshift distribution of Ly α forest clouds at high z revealed that the metal-poor population was much less clustered than the present-day galaxies (Sargent et al. 1980). Furthermore, there were suggestions that the Ly α forest might be an entirely separate population from the absorbers at larger column density ($N_{H\text{I}} \geq 10^{17} \text{ cm}^{-2}$), which have associated metal-line absorption and cluster like galaxies (Sargent, Boksenberg, & Steidel 1988; Tytler 1987). Proposed explanations of a non-galactic Ly α forest include pressure-confined clouds in the IGM (Sargent et al. 1980; Ikeuchi & Turner 1991) and CDM minihalos (Ikeuchi 1986; Rees 1986). Recent results from the HIRES spectrograph on the Keck 10m telescope still admit the possibility of a dual-population (galactic and intergalactic) Ly α forest. Highly resolved metal-line absorption in high- z damped-Ly α systems appears to originate in thick, rapidly rotating ($\gtrsim 200 \text{ km s}^{-1}$) protogalactic disks (Prochaska & Wolfe 1997). The mean metallicity of high- z Ly α clouds declines sharply at low column densities, from $[\text{C}/\text{H}] \simeq -2.5$ at $N_{H\text{I}} \geq 10^{14.5} \text{ cm}^{-2}$ to an upper limit of $[\text{C}/\text{H}] < -3.5$ for $10^{13.5} < N_{H\text{I}} < 10^{14} \text{ cm}^{-2}$ (Lu et al. 1998).

With the *HST* discovery of several $z \leq 0.16$ Ly α clouds along the 3C 273 sightline (Morris et al. 1991; Bahcall et al. 1991), it was now possible with pencil-beam redshift surveys to search for far less luminous galaxies coincident in redshift space with the low column density absorbers. Morris et al. (1993) completed a $B \sim 19$ survey of ~ 4 square degrees around 3C 273 that detected no galaxies within $1.5h^{-1}$ Mpc of any absorber. They concluded that the absorption is extragalactic in origin. A further deep imaging survey of $53' \times 52'$ around 3C 273 by Rauch, Weymann, & Morris (1996) to a limiting central surface brightness of $\mu_r = 26.4$ revealed no low surface brightness galaxies within projected separations of $80h^{-1}$ kpc and $123h^{-1}$ kpc, respectively, at the two nearest absorber redshifts.

Lanzetta et al. (1995), on the basis of an $r < 21.5$ survey within $1'.3$ of several *HST*/FOS target QSOs (Bahcall et al. 1993), concluded instead that the Ly α forest is largely due to extended galactic gaseous halos (Bahcall & Spitzer 1969) or gaseous disks (Maloney 1993; Hoffman et al. 1993) of size $\approx 160h^{-1}$ kpc and roughly unit covering factor. Their survey spanned a much greater cumulative pathlength, $\Delta z \approx 2.86$, than the $\Delta z \approx 0.16$ sampled by the Morris et al. (1993) study of the 3C 273 foreground. Lanzetta et al. detected 30 galaxies at impact

parameters $\lesssim 160h^{-1}$ kpc from the QSO lines of sight (LOS), closer than any detected galaxy to the 3C 273 LOS. They found: (1) a strong increase in the probability of a galaxy-absorber association for galaxy impact parameters under $160h^{-1}$ kpc. They also noted a statistical anti-correlation between the equivalent width of Ly α absorption and the impact parameter of a galaxy-absorber pair. They argue that at $z \lesssim 1$, the fraction of Ly α absorption systems arising in galactic halos is at least 0.35 ± 0.10 , and probably 0.65 ± 0.18 . It is noteworthy that their *HST*/FOS Ly α absorber sample was limited to equivalent widths $W_{\text{Ly}\alpha} \gtrsim 0.3\text{\AA}$, larger than almost all the *HST*/GHRS detections and probably not representative of the extremely metal-poor population, with $N_{\text{HI}} < 10^{14} \text{ cm}^{-2}$. Mo and Morris (1994) used Monte Carlo simulations to show that the galactic-halo fraction of 3C 273 absorbers, all with $N_{\text{HI}} \lesssim 10^{14} \text{ cm}^{-2}$, could only be $\approx 20\%$ given the observed number of absorbers and the weak correlation between absorbers and galaxies on large scales.

In a different approach, Shull, Stocke, & Penton (1996, hereafter SSP96; Stocke, Shull, & Penton 1995) obtained *HST*/GHRS spectra of four nearby bright AGNs within the boundaries of existing wide-angle redshift surveys to determine whether Ly α absorbers nearby are correlated with large-scale structure, as first suggested by Oort (1981). They detected a total of 11 Ly α absorbers along these sightlines within a GHRS wavelength range corresponding to $1500 \lesssim cz \lesssim 10500 \text{ km s}^{-1}$. Using the wavelet analysis of Slezak, de Lapparent, & Bijaoui (1993) to subdivide their AGN sightlines into “void” and “supercluster” regions, SSP96 found four of their eleven absorbers in voids. Because their sightlines probed an approximately equal pathlength of void and supercluster, binomial statistics gave a fair probability (19%) that the $z < 0.035$ absorbers are uniformly distributed and not biased towards superclusters. From the relation between Ly α equivalent widths and nearest-galaxy distance, SSP96 argue that the $W_{\text{Ly}\alpha} < 0.1\text{\AA}$ absorbers are distributed in a manner statistically indistinguishable from clouds randomly placed with respect to galaxies. Although the nearest-galaxy distances of their $W_{\text{Ly}\alpha} > 0.1\text{\AA}$ subsample are broadly consistent with the Lanzetta et al. (1995) trend extended to larger impact parameters ($\gtrsim 500h^{-1}$ kpc), it is unlikely that the Ly α absorbers could be physically associated with galaxies at that separation.

We use the large-scale smoothed galaxy number density to compare the distribution of $z < 0.035$ Ly α absorbers with that of typical luminous galaxies. Whereas SSP96 identified the absorbers as either “void” or “supercluster”, we quantify the large-scale structure in the vicinity of the absorbers. The smoothed galaxy density field is a more robust indicator of absorber environment than the

nearest-galaxy distance, particularly on scales larger than 1 Mpc.

The technique we develop requires a wide-angle redshift survey overlapping the AGN sightlines of interest and adequately sampling the galaxy population at the Ly α absorber redshifts. Thus we restrict ourselves to the $cz < 10500$ km s $^{-1}$ absorbers along the sightlines to 3C 273 and the four AGNs of SSP96. For the 18 Ly α absorbers meeting these specifications, we use the galaxy number density field from the CfA2 Redshift Survey (Geller & Huchra 1989; Vogeley et al. 1994; Marzke, Huchra, & Geller 1994, hereafter MHG94) and adjacent regions also surveyed to $m_{Zw} = 15.5$ (Marzke et al. 1996; Grogin, Geller, & Huchra 1998). Even with this modest sample of absorbers, we obtain rather tight constraints on the relation between the local Ly α absorbers and the large-scale structure marked by intrinsically luminous galaxies.

Section 2 describes the nearby Ly α absorption systems and the galaxy redshift surveys surrounding them. Section 3 describes the density estimation technique and shows maps of the galaxy density field toward the five target AGNs. We also derive the cumulative distribution function (CDF) of the densities around the 18 Ly α absorption systems. In §4 we investigate the implications of the Ly α density CDF by comparing it with CDFs for several test populations. We also compute likelihood intervals for models of the absorbers’ spatial distribution. We address sources of uncertainty in §5, and estimate the improved constraints likely with a larger sample of nearby Ly α absorbers. We conclude in §6.

2. Data

2.1. Lyman-alpha Absorption Systems

Our sample of local Ly α absorbers comprises seven systems with $cz < 10500$ km s $^{-1}$ detected towards 3C 273 (Morris et al. 1993) and eleven systems detected in the sightlines toward the AGN Mrk 335, Mrk 421, Mrk 501, and I Zw 1 (SSP96). The 3C 273 observations extend down to 1215Å (Weymann et al. 1995) and include Ly α forest systems well into the damping wing of Galactic Ly α absorption. The AGN observations span a more limited wavelength range of 1222Å–1259Å, corresponding to a redshift window of $1500 \lesssim cz \lesssim 10500$ km s $^{-1}$ for the detection of Ly α absorption systems. Three of the four AGN have $cz < 10500$ km s $^{-1}$, further reducing the path length probed by these sightlines. Table 1 summarizes the relevant data for each of the Ly α sources, including the source redshift and the redshift range for absorber detection. In Table 2 we list the redshifts and equivalent widths for the 18 Ly α absorbers.

2.2. Redshift Surveys

The CfA2 Redshift Survey (Geller & Huchra 1989) provides the broad sky coverage and dense sampling necessary to evaluate the galaxy number density, smoothed on scales $\lesssim 5h^{-1}$ Mpc, around Ly α absorbers with $cz \lesssim 10000$ km s $^{-1}$. Although there have been much deeper, pencil-beam surveys along QSO sightlines (Morris et al. 1993; Lanzetta et al. 1995) to link Ly α absorption with specific galaxies, these subtend much too small an angle to evaluate nearby densities on $5h^{-1}$ Mpc scales. SSP96 chose their four AGN partly because they are within the CfA2 boundaries as analyzed by Vogeley et al. (1994) and MHG94: $8^{\text{h}} \leq \alpha \leq 17^{\text{h}}$, $8^{\circ}5 \leq \delta \leq 44^{\circ}5$ (CfA2 North) and $20^{\text{h}} \leq \alpha \leq 4^{\text{h}}$, $-2^{\circ}5 \leq \delta \leq 42^{\circ}$ (CfA2 South). Redshifts around these four AGN sightlines are contained in Huchra et al. (1990), Huchra, Geller, & Corwin (1995), Huchra, Vogeley, & Geller (1998), and are available through NED¹.

We have also surveyed a $2^{\text{h}} \times 12^{\circ}$ region nearly centered on 3C 273 (Grogin, Geller, & Huchra 1998). With ≈ 1060 redshifts in the region $11^{\text{h}}30^{\text{m}} \leq \alpha \leq 13^{\text{h}}30^{\text{m}}$ and $-3^{\circ}5 \leq \delta \leq 8^{\circ}5$, this survey extension is 99.5% complete to the CfA2 magnitude limit ($m_{\text{Zw}} = 15.5$) and 98.1% complete to the Zwicky catalog limit ($m_{\text{Zw}} = 15.7$). This additional survey yields estimates of the global density at the locations of the 3C 273 Ly α absorbers. In addition to the 3C 273 field redshifts, we also incorporate ~ 1700 Zwicky galaxy redshifts at low Galactic latitude from the Galactic Plane Survey by Marzke, Geller, & Huchra (1996). These additional redshifts outside the CfA2 boundaries prevent substantial underestimation of the galaxy density at locations within a smoothing length of the survey boundaries.

3. Estimating the Smoothed Galaxy Number Density

Our goal is to compare the distribution of Ly α absorbers with the large-scale distribution of galaxies. If the absorbers sample the large-scale structure marked by luminous galaxies in a redshift survey, the distribution of smoothed galaxy number densities around the absorbers should be consistent with the distribution of densities around survey galaxies. Conversely, if the Ly α absorbers arise in a host population distributed independently of the large-scale structure, the densities around the absorbers should resemble the densities around similarly distributed locations in the survey volume.

¹The NASA/IPAC Extragalactic Database (NED) is operated by the Jet Propulsion Laboratory, California Institute of Technology, under contract with the National Aeronautics and Space Administration.

In §3.1 we describe the smoothed galaxy number density field constructed from the redshift survey data of §2.2. We show maps of the density field towards five AGN with low-redshift Ly α absorbers in §3.2. Finally we combine the densities at each of the 18 absorber locations into a cumulative distribution function (§3.3) for comparison with density CDFs of various test populations in §4.

3.1. Method

To evaluate the galaxy density around the local Ly α absorbers, we first transform the point distribution of the CfA2 Survey into a continuously defined number density field throughout redshift space. We smooth each galaxy in redshift space by a unit-normalized Gaussian kernel W of width $\sigma = 5h^{-1}$ Mpc:

$$W(\mathbf{x} - \mathbf{x}_{\text{gal}}) = (2\pi\sigma)^{-3/2} \exp\left(-|\mathbf{x} - \mathbf{x}_{\text{gal}}|^2 / 2\sigma^2\right). \quad (3-1)$$

We choose a $5h^{-1}$ Mpc smoothing length to coincide with the galaxy-galaxy correlation length (Peebles 1993; Marzke et al. 1995; Jing, Mo, & Boerner 1998) and with the pairwise velocity dispersion in the survey (Marzke et al. 1995). In §5.2 we discuss the sensitivity of our results to this choice.

We make no attempt to remove peculiar velocity distortions (cluster “fingers”, etc.) from the redshift survey or from the Ly α absorber velocities. In principle, they should share the same local velocity field. We do introduce the standard heliocentric to Galactocentric correction,

$$cz = cz_{\odot} + (300 \text{ km s}^{-1}) \sin l \cos b, \quad (3-2)$$

for an object at Galactic longitude l and latitude b . We place each object at a comoving distance r appropriate for a $q_0 = 0.5$ universe with pure Hubble flow:

$$r(z) = \left(\frac{2c}{H_0}\right) \left[1 - (1+z)^{-1/2}\right]. \quad (3-3)$$

We thus underestimate spatial overdensities associated with clusters, which are broadened in the radial direction. Our smoothing kernel effectively washes out peculiar velocities $\lesssim 500 \text{ km s}^{-1}$, close to the $540 \pm 180 \text{ km s}^{-1}$ pairwise velocity dispersion measured by Marzke et al. (1995) for the combined CfA2 and SSRS2 (da Costa et al. 1994) surveys.

Because the CfA2 Redshift Survey is flux-limited, an increasing fraction of the galaxies at larger redshift fall below the magnitude limit and do not appear in the survey. In computing the density field, we compensate for the magnitude-limited

sample by assigning each galaxy a weight $1/\psi$, where the selection function ψ is

$$\psi(\alpha, \delta, z) = \frac{\int_{-\infty}^{M_{\text{lim}}(\alpha, \delta, z)} \phi(M) dM}{\int_{-\infty}^{M_{\text{cut}}} \phi(M) dM}. \quad (3-4)$$

Here M_{lim} is the effective absolute magnitude limit at the galaxy position and $\phi(M)$ is the differential luminosity function (LF). For $M_{\text{lim}} \geq M_{\text{cut}}$, we assign galaxies unit weight. All magnitudes are Zwicky magnitudes. Numerical values for absolute magnitudes implicitly include the h -dependence in equation (3-3).

MHG94 fit the CfA2 LF to a Schechter function ϕ_{SF} (Schechter 1976), convolved with a Gaussian error of $\sigma_M = 0.35$ mag (Huchra 1976) in the Zwicky magnitudes:

$$\begin{aligned} \phi_{\text{SF}}(M) &= \phi_* (0.4 \ln 10) 10^{0.4(M_* - M)(1 + \alpha)} \exp \left[-10^{0.4(M_* - M)} \right]; \\ \phi_{\text{CfA2}}(M) &= \frac{1}{\sqrt{2\pi}\sigma_M} \int_{-\infty}^{\infty} \phi_{\text{SF}}(M') \exp \left[-(M' - M)^2 / 2\sigma_M^2 \right] dM'. \end{aligned} \quad (3-5)$$

We adopt the values $\phi_* = 0.04 (\text{Mpc}/h)^{-3}$, $M_* = -18.8$, and $\alpha = -1.0$ found by MHG94 using $M_{\text{cut}} = -16.5$. We discuss the sensitivity of our results to the LF parameters in §5.1. For computational convenience in determining ψ , we replace the convolution of equation (3-5) with $\phi_{\text{CfA2}}(M) \approx \phi_{\text{SF}}(M + 0.1 \text{ mag})$. This approximation recovers the true ψ to better than 5% for $cz \lesssim 12000 \text{ km s}^{-1}$.

For a galaxy at position (α, δ) and at luminosity distance $D_L(z) = (1+z)r(z)$, we estimate M_{lim} according to

$$M_{\text{lim}}(\alpha, \delta, z) = m_{\text{lim}} - 5 \log \left[\frac{(1+z)r(z)}{1h^{-1} \text{ Mpc}} \right] - 25 - \Delta m_{\text{K}}(z) + \Delta m_{\text{ext}}(\alpha, \delta). \quad (3-6)$$

In equation (3-6), m_{lim} is the CfA2 flux limit, Δm_{K} is a K -correction, and Δm_{ext} is a correction for Galactic extinction. Photoelectric photometry of Zwicky galaxies (Takamiya, Kron, & Kron 1995) suggests that Volume I of the Zwicky catalog (Zwicky et al. 1961–1968) goes ≈ 0.4 mag fainter than the other volumes at the CfA2 magnitude limit, $m_{\text{Zw}} = 15.5$. To correct for this Volume I scale error, we adopt $m_{\text{lim}} = 15.9$ for all galaxies with $\delta \leq 14^\circ 5$ in CfA2 North and the 3C 273 region extension.

Lacking morphological types for the majority of CfA2, we apply a generic K -correction, $\Delta m_{\text{K}}(z) = 3z$, appropriate for type Sab (Pence 1976). Our error in the K -correction will be small due to the predominantly low redshifts ($z \lesssim 0.05$) in the survey. To obtain our correction $\Delta m_{\text{ext}}(\alpha, \delta)$ for Galactic extinction along

a particular line of sight, we first interpolate the HI map of Stark et al. (1992). We then convert from HI to reddening with the relation $\langle N(\text{HI})/E(B-V) \rangle = 4.8 \times 10^{21} \text{ cm}^{-2} \text{ mag}^{-1}$ (Zombeck 1990), and adopt a standard extinction law $\Delta m_{\text{ext}} \equiv A_B = 4.0E(B-V)$.

We compute the smoothed galaxy number density n at a given point $\mathbf{r} \equiv (\alpha, \delta, r(z))$ by summing the contributions from all i galaxies in the survey:

$$\begin{aligned} n(\mathbf{r}) &= \sum_i \frac{W(\mathbf{r} - \mathbf{r}_i)}{\psi_i} \\ &= \sum_i \frac{W(\mathbf{r} - \mathbf{r}_i) \int_{-\infty}^{M_{\text{cut}}} \phi(M) dM}{\int_{-\infty}^{M_{\text{lim}}(\mathbf{r}_i)} \phi(M) dM} \\ &= \bar{n} \sum_i \frac{W(\mathbf{r} - \mathbf{r}_i)}{\int_{-\infty}^{M_{\text{lim}}(\mathbf{r}_i)} \phi(M) dM}. \end{aligned} \tag{3-7}$$

For the CfA2 Survey, MHG94 derive a mean density $\bar{n} \equiv \int_{-\infty}^{M_{\text{cut}}} \phi(M) dM = 0.07 (\text{Mpc}/h)^{-3}$ with $M_{\text{cut}} = -16.5$. This analysis yields a distribution of dimensionless galaxy density contrasts, $n(\mathbf{r}_i)/\bar{n}$, at the absorber positions \mathbf{r}_i which may be compared with the n/\bar{n} distribution of various control samples.

3.2. CfA2 Density Maps toward Local Lyman-alpha Systems

For each of the five sources in Table 1, we display the results of our density mapping in two forms. The first representation is similar to the standard “wedge plot” format for redshift survey data: we project galaxy positions over a narrow declination range onto a circular section with R.A. as the azimuth coordinate and redshift as the radial coordinate. We add the density contrast as a superposed isodensity contour map, made by sampling the density at regular $3h^{-1}$ Mpc intervals on the midplane (or, more accurately, the mid-cone) of the wedge plot.

We set the outer boundary of the wedge plots at 15000 km s^{-1} , well into the region where shot noise dominates the density estimate. We choose a “thickness” of six degrees in declination, centered on each LOS. Our $5h^{-1}$ Mpc density smoothing length subtends this angle at a redshift of $\approx 5000 \text{ km s}^{-1}$. For $cz \gtrsim 5000 \text{ km s}^{-1}$, there is density variation with declination that is lost in projection. To showcase the large-scale structure toward each target, the wedge plots have a 30° opening angle centered on each LOS, corresponding to $(2^h/\cos\delta)$ of right ascension at the central declination δ . Our density smoothing length subtends this angle at a redshift of $(1000/\cos\delta) \text{ km s}^{-1}$. We accommodate the

dynamic range of the density map with underdensity contours (dotted) in linear decrements of $0.2\bar{n}$ and overdensity contours (solid) in logarithmic increments corresponding to \bar{n} , $2\bar{n}$, $4\bar{n}$, $8\bar{n}$, etc. In addition to the surveyed galaxies (small squares), we also plot the locations of the detected Ly α absorbers (large triangles) along the line of sight (dashed) to the background source (large circle, if $cz_{\text{src}} \leq 15000 \text{ km s}^{-1}$).

For the second display, we sample the density at 100 km s^{-1} radial intervals for $cz \leq 15000 \text{ km s}^{-1}$ along the line of sight to the selected background source. We then plot the density profile (n/\bar{n}) along the LOS (dashed curve) versus redshift. We indicate the redshifts of the detected Ly α absorbers (dotted lines) as well as the redshift interval over which the absorbers could have been detected (solid lines). If the upper redshift limit coincides with the source of Ly α emission, we indicate this coincidence with a doubled solid line. Within this redshift interval, we also show the $\pm 1\sigma$ uncertainty in the local density estimate (solid curves). This density error estimate is the quadrature sum of the fractional errors due to sampling variance (cf. §5.3) and the uncertain survey LF (cf. §5.1).

3.2.1. 3C 273

For the wedge plot of the 3C 273 region (Figure 1), we center the right ascension on the $11^{\text{h}}5-13^{\text{h}}5$ range of the CfA2 survey extension (Grogin, Geller, & Huchra 1998) instead of the $\pm 15^\circ$ about 3C 273 ($\alpha = 12^{\text{h}}26^{\text{m}}6$). Because the survey extension is complete to the Zwicky catalog limit, $m_{\text{Zw}} = 15.7$, we also show the locations of the fainter galaxies (small crosses) to compare with the Ly α systems. We use only the brighter $m_{\text{Zw}} \leq 15.5$ galaxies to derive the density estimate. The uncertainty in the density estimator rises dramatically for $cz \gtrsim 12000 \text{ km s}^{-1}$ (cf. 5.3), and exceeds ± 1 dex at the two absorption systems near 15000 km s^{-1} . We therefore only consider the 3C 273 absorbers with $cz \leq 10500 \text{ km s}^{-1}$, coincident with the velocity maximum for the other AGN lines of sight.

The seven 3C 273 absorbers with $cz \leq 10500 \text{ km s}^{-1}$ inhabit a wide range of environments. The two nearest Ly α systems are near the Virgo cluster, and thus are difficult to identify in the crowded wedge plot. Their redshifts are clearly indicated in the associated density profile. These two systems inhabit some of the highest-density regions in the LOS. In contrast, two of the other absorbers inhabit the low-density extreme of the LOS, a large void at $cz \approx 9500 \text{ km s}^{-1}$.

3.2.2. Mrk 335

Figure 2 shows the Mrk 335 region. The local galaxy densities at the Ly α absorber locations span the density range in the LOS redshift window, including a pair with $cz \approx 2350 \text{ km s}^{-1}$ near the density minimum.

3.2.3. Mrk 421

Figure 3 shows the Mrk 421 region. This LOS is intriguing in that only one absorber appears within the $\approx 7500 \text{ km s}^{-1}$ sensitivity window; it resides in a relatively underdense environment.

3.2.4. Mrk 501

The proximity of Mrk 501 ($\alpha = 16^{\text{h}}52^{\text{m}}2$) to the CfA2 North boundary at 17^{h} poses an added challenge to determination of the densities surrounding its Ly α absorbers. Fortunately there is an essentially complete redshift survey (Marzke et al. 1996) beyond this boundary, mitigating edge effects on the density estimate. In the region $17^{\text{h}} \leq \alpha \leq 18^{\text{h}}$ and $+34^\circ \leq \delta \leq +46^\circ$, there are redshifts for 140 of the 150 Zwicky galaxies with $m_{\text{Zw}} \leq 15.5$.

Rather than cropping the Mrk 501 wedge plot at the CfA2 survey boundary, we set the upper R.A. limit in Figure 4 at 18^{h} in order to show the large-scale structure east of the LOS. As noted above, there are redshifts for more than 90% of the galaxies in the plotted region with $\alpha > 17^{\text{h}}$. We therefore have high confidence in the density estimates along the Mrk 501 LOS.

Interestingly, there are no absorbers in the region of large overdensity beyond $cz \simeq 8000 \text{ km s}^{-1}$ associated with the Hercules supercluster. On the contrary, two of the absorbers are near the LOS density minimum, in a foreground void to the supercluster. A third is on the outskirts of this void, in a region of middling density.

3.2.5. I Zw 1

Figure 5 shows the I Zw 1 region. The two nearest absorption systems are located in a relatively shallow void; the third system appears to be associated with the galaxy wall behind it at $cz \approx 5500 \text{ km s}^{-1}$. Beyond this wall, the LOS passes through a larger and emptier void containing no detected Ly α systems.

3.3. Density Distribution for the Lyman-Alpha Absorber Sample

Figure 6 shows the cumulative distribution function (CDF) of the densities surrounding the 18 Ly α absorbers (solid). We plot the density contrast (n/\bar{n}) on a logarithmic axis. Error in the overall normalization of (n/\bar{n}) translates all CDFs along the x-axis but does not change their shape. The distribution of (n/\bar{n}) for the Ly α absorbers is broad, with fully half the absorbers in substantially underdense regions of the survey: (n/\bar{n}) < 0.4. This considerable fraction of low- (n/\bar{n}) absorption systems is the principal discriminant among the density CDFs of test samples in §4.

4. Interpretation

To understand the physical implications of the galaxy density distribution around the sample of nearby Ly α absorption systems, we define several test populations. We then calculate the local densities surrounding each of the locations in the test samples. Finally, we employ a two-population Kolmogorov-Smirnov (K-S) statistic to compare the galaxy number density distribution of the Ly α absorbers with the density distributions from the test samples of: (1) CfA2 galaxies (§4.1, §4.2) and (2) randomly selected locations within the redshift survey boundaries (§4.3). To construct these test samples, we must also simulate the radial sampling bias caused by the redshift windows of the Ly α forest observations (Table 1).

4.1. Comparison with All CfA2 Galaxies

For this test sample, we determine the density contrast (n/\bar{n}) at the locations of each CfA2 galaxy (within the boundaries listed in §2.2 and including the 3C 273-region extension). To account for the radial sampling bias of the Ly α sight-lines, we assign each of the densities in the sample a weight W equal to the number of redshift intervals in Table 1 which contain the redshift of the corresponding galaxy. The value of W therefore varies between zero ($cz > 10660$ km s $^{-1}$) and five ($1713 < cz < 7901$ km s $^{-1}$).

When using CfA2 galaxies to trace the density field, the survey magnitude limit causes an additional radial sampling bias. Even though we have corrected for the survey selection function ψ in determining (n/\bar{n}), the CfA2 galaxies at larger redshifts are sampling (n/\bar{n}) much more sparsely because we see proportionately fewer of them per unit volume. We attempt to correct for this sampling bias by assigning (n/\bar{n}) for each galaxy an additional weighting factor of $1/\psi$.

Thus each (n/\bar{n}) in the sample has weight (W/ψ) .

The weighting is not an entirely satisfactory solution to the radial bias problem, because the unseen fraction $(1 - \psi)$ of galaxies at higher redshift are not all located at the positions of the observed fraction ψ . The fixed smoothing length of the density estimator results in pronounced local maxima in the density field at the locations of higher-redshift galaxies in the survey. We therefore tend to overestimate the high-density end of the (n/\bar{n}) distribution when assuming that a particular galaxy's (n/\bar{n}) is representative of its $(\psi^{-1} - 1)$ unseen neighbors.

Figure 6 shows the cumulative distribution function (CDF) of (n/\bar{n}) for all CfA2 galaxies, with (W/ψ) -weighting (dotted) as well as with W -weighting alone (dashed). For comparison, we also plot the density CDF for the Ly α absorbers (solid). Clearly the Ly α absorbers occur far more frequently in underdense regions. The K-S probability that the Ly α CDF and the (W/ψ) -weighted galaxy CDF are drawn from the same underlying distribution is only 3×10^{-8} , a 5.1σ rejection of the null hypothesis. The K-S probability for the W -weighted CDF is 9×10^{-4} , a 3.3σ rejection.

4.2. Comparison with CfA2 Galaxies in Random LOS Cylinders

The *HST* observations of local Ly α absorbers sample the population along narrow sightlines through redshift space. This geometric sampling is not reproduced in the volume-filling, complete CfA2 galaxy sample (§4.1). Discrete lines of sight through the survey are less likely to sample rich galaxy clusters because the clusters within $\sim 100h^{-1}$ Mpc cover only a small fraction of the sky. We therefore define another test population by selecting random LOS through the CfA2 survey and extracting the galaxies within cylinders of diameter $5h^{-1}$ Mpc (the density smoothing length) around those LOS.

For each of the five actual AGN sightlines (Table 1), we assign the corresponding redshift interval to one fifth of the randomly generated LOS cylinders. To obtain a suitably large test sample of 5000 galaxies, we use ~ 150 LOS. We again correct for the selection function sampling bias (cf. §4.1) by assigning each galaxy's (n/\bar{n}) value a ψ^{-1} weight in the census.

Figure 7 shows the CDF of (n/\bar{n}) for the random-LOS CfA2 galaxies, ψ^{-1} -weighted (dotted) as well as unit-weighted (short dash). We again see a disparity between the Ly α and CfA2 galaxy CDFs, though perhaps less pronounced than for the full-CfA2 sample. The sharp rise in the unit-weighted CDF at $(n/\bar{n}) \approx 4$ is caused by a combination of: (1) a preponderance of Virgo cluster galaxies, all at $(n/\bar{n}) \approx 4$, appearing in the one-fifth of LOS cylinders which extend to

$z = 0$ and (2) a lack of $(n/\bar{n}) > 4$ galaxies because of the low probability that a $5h^{-1}$ Mpc cylinder intersects a CfA2 cluster (other than Virgo), or even a galaxy with $cz \gtrsim 8000 \text{ km s}^{-1}$. This feature is much less apparent after we apply the selection-function weighting correction.

The K-S probability that the Ly α CDF and the ψ^{-1} -weighted galaxy CDF are drawn from the same underlying distribution is 3×10^{-5} , a 4.2σ rejection. The K-S probability for the unit-weighted CDF is 2×10^{-4} , a 3.7σ rejection.

4.3. Comparison with Randomly Generated Velocities along Random LOS

We next construct test populations of Ly α absorption systems with randomly chosen redshift-space coordinates along randomly selected LOS. We first adopt a constant linear density $N_{\text{Ly}\alpha}(cz) = 1/(2500 \text{ km s}^{-1})$ for our mock absorbers, roughly equivalent to the observed mean incidence for the five selected *HST* lines of sight (18 absorbers over $\sim 42000 \text{ km s}^{-1}$). Because all these sightlines have $z_{\text{max}} < 0.04$ and span a redshift range $\Delta z \approx 0.03$, we ignore the linear density gradient $dN_{\text{Ly}\alpha}(z)/dz$. As in the previous case, we assign radial intervals to these random LOS by selecting evenly from the five redshift windows of Table 1.

4.3.1. Single-population Model

For a given random LOS through CfA2, we sample the smoothed galaxy density at $1h^{-1}$ Mpc radial intervals to obtain a density-vs.-redshift profile $n(z)$. We take this density profile, raised to an exponent β , as the probability distribution function for the mock-Ly α redshifts:

$$P(z) dz = \frac{n^\beta(z) dz}{\int_{z_{\text{min}}}^{z_{\text{max}}} n^\beta(z') dz'}. \quad (4-1)$$

By drawing a sample of mock absorbers from a $\beta = 0$ (or $P(z) = \text{const.}$) model, we can test the hypothesis that low column-density Ly α absorbers are distributed uniformly throughout space and completely uncorrelated with local galaxy density. Similarly, we could test the hypothesis that the Ly α systems reside in density environments typical of CfA2 galaxies by drawing a sample of mock absorbers from a $\beta = 1$ model.

The distribution power-law index β may be viewed very roughly as the combination of a cloud-creation index β_c and a cloud-destruction index β_d . When

mergers, etc., destroy low column-density absorbers in regions of high galaxy density ($\beta_d > 0$), we might expect an *anticorrelation* of absorber location with local galaxy density ($\beta < 0$). To estimate β in a merger-destruction scenario, we note that the rate of cloud-galaxy interactions scales as the product of the local galaxy cross section ($\propto n$) and the peculiar velocity of the clouds through the redshift space ($\propto n^{1/2}$). If the clouds were produced in direct proportion to the local galaxy density ($\beta_c = 1$), then $\beta_d \approx 3/2$ would imply $\beta \approx -1/2$.

Only in the case $\beta = 0$ do we explicitly simulate a sample of ≈ 5000 mock absorbers to compare with the observed set of Ly α absorbers. Figure 7 shows the density CDF of the 5000 randomly located absorbers (long dash), which may be compared with the CDF for the observed Ly α systems (solid). The agreement between the two CDFs is remarkable, particularly when compared with the CfA galaxy CDFs in Figs. 6 and 7. The K-S probability that the observed Ly α densities share the same underlying distribution as the $\beta = 0$ model is 0.20, consistent at the 1.3σ level. This probability only varies by ± 0.01 for multiple realizations of the randomly generated sample, indicating that a 5000-member sample is sufficiently large for our analysis.

We check the sensitivity of this result to the adopted linear density of randomly generated absorbers. When we vary the linear density by $\pm 30\%$, the K-S probability varies by ± 0.03 , larger than the sampling variance (0.01) but still statistically insignificant. We also test a simulation in which the redshift interval *and* the linear density of absorbers along a random sightline are set to the observed values for one of the five AGN sightlines. This sampling compensates for varying sensitivity for Ly α detection between sightlines. The analyses of the 3C 273 *HST* spectra yielded detections of lower equivalent-width absorption ($\gtrsim 30$ mÅ) features than SSP96 detected for their AGN. Not surprisingly the 3C 273 LOS has a significantly higher linear density of absorbers (cf. Tables 1 and 2). The K-S probability for this variable-linear-density model is the same as the 0.20 probability for the fixed-density model to within the sampling variance. The match between the density CDFs of the observed Ly α clouds and the randomly chosen locations in redshift space is robust against reasonable variation in the adopted linear density of mock absorbers.

We next use a maximum-likelihood technique to estimate the range of β consistent with the observed density distribution of local Ly α systems. If equation (4-1) describes the actual redshift distribution of local Ly α absorbers, then the likelihood of seeing the observed redshift distribution (Table 2) is the product of

the individual probabilities for each absorber at \mathbf{r}_i :

$$\mathcal{L}(\beta) = \prod_i P(\mathbf{r}_i; \beta) = \prod_i \frac{n^\beta(\mathbf{r}_i)}{\int_{z_{i,\min}}^{z_{i,\max}} n^\beta(\alpha_i, \delta_i, z') dz'} \quad (4-2)$$

Given the prior assumption that the underlying distribution of Ly α locations follows a β -model, then the quantity $-2 \ln[\mathcal{L}(\beta)]$ should be distributed as χ^2 in β .

In Figure 8, the solid curve shows the model likelihood for the range $-1.5 \leq \beta \leq 1.5$. We obtain a maximum likelihood value of $\beta = -0.02 \pm 0.23$ from the 18 nearby Ly α systems. A single-population Ly α forest that traces the local large-scale structure ($\beta = 1$) is inconsistent with our result at the 4σ level. This result may be compared with the $\sim 4\sigma$ inconsistencies between the density CDFs of the Ly α absorbers and the galaxy test populations (§§4.1, 4.2), which should have a $\beta = 1$ distribution throughout the survey.

4.3.2. Dual-population Model

Mo and Morris (1994) speculated that the Ly α absorbers may include two distinct populations: one population associated with the gaseous extended halos of galaxies, and another population of isolated, unclustered clouds. In this model, we might expect the galactic-halo fraction f_{gal} to have local densities consistent with the densities around typical galaxies in the survey ($\beta = 1$) and the unclustered fraction to have local densities consistent with randomly chosen locations in the survey ($\beta = 0$). Equation (4-1) then yields a distribution function of dual-population absorbers of the form:

$$P(z) dz = \frac{f_{\text{gal}} n(z) dz}{\int_{z_{\min}}^{z_{\max}} n(z') dz'} + \frac{(1 - f_{\text{gal}}) dz}{(z_{\max} - z_{\min})}. \quad (4-3)$$

In analogy with equation (4-2) we can define a likelihood function for the observed clouds to be drawn from a model with galactic fraction f_{gal} :

$$\mathcal{L}(f_{\text{gal}}) = \prod_i P(\mathbf{r}_i; f_{\text{gal}}), \quad (4-4)$$

where P is now given by equation (4-3).

In Figure 9, the solid curve shows the likelihood of a dual population model with fraction f_{gal} distributed like the CfA2 galaxies ($\beta = 1$) and the remainder

distributed uniformly ($\beta = 0$). The maximum-likelihood value for the galactic-type fraction is $f_{\text{gal}} = 0.00$, with a 1σ upper limit of $f_{\text{gal}} = 0.24$. This result is inconsistent at a 99% (2.6σ) confidence level with the upper estimate of $f_{\text{gal}} \approx 0.65$ given by Lanzetta et al. (1996). Their lower limit of $f_{\text{gal}} \approx 0.38$ is only excluded at a confidence level of 88% (1.5σ).

5. Discussion

Our Ly α local density analysis suffers from a number of sources of uncertainty which increase the error bars in our results of §4. Because we assign each galaxy a weight derived from the CfA2 selection function, the density estimator is sensitive to uncertainty in the shape of the CfA2 luminosity function. The density estimator, constructed from a point distribution of galaxies, is subject to increasing shot noise at larger redshift. The shot noise dominates at $cz \gtrsim 10000 \text{ km s}^{-1}$, where the mean distance between survey galaxies rapidly exceeds our $5h^{-1} \text{ Mpc}$ smoothing length. For this reason, we may worry that the parameter constraints are also sensitive to the adopted smoothing length. Here we quantify some of these sources of uncertainty and estimate the improvements in Ly α distribution constraints which would result from a larger sample of nearby absorbers.

5.1. Uncertainty in the CfA2 Luminosity Function

The uncertainty in the CfA2 luminosity function (MHG94) introduces an uncertainty in our selection function weighting (eq. 3-4). Our results for β and f_{gal} are insensitive to the overall LF normalization, ϕ_* ; it cancels out of equations (4-1) and (4-3). We may therefore restrict our error analysis to uncertainty in the LF shape parameters, α and M_* . To incorporate this LF uncertainty into our error bars on β and f_{gal} , we Monte Carlo resample the densities in equations (4-1) and (4-3), varying the LF parameters according to their ranges from MHG94: $M_* = -18.8 \pm 0.3$, and $\alpha = -1.0 \pm 0.2$. The 1σ bounds on the absorber distribution parameters increase only marginally from §4:

$$\beta : -0.02 \pm 0.23 \rightarrow -0.02 \pm 0.24; \quad f_{\text{gal}} : 0.00_{-0}^{+0.24} \rightarrow 0.00_{-0}^{+0.25}. \quad (5-1)$$

MHG94 show that the respective LFs of CfA2 North and CfA2 South differ significantly ($> 2\sigma$) with the LF of the Combined (CfA2 North+South) sample. This North/South LF difference is difficult to interpret; it may be caused by large-scale systematic errors in the Zwicky photometry or by real variations in the underlying LF across the survey volume. We investigate its effect on our

density distribution analysis by replacing the selection function derived from the Combined sample ($\phi_* = 0.04 \text{ (Mpc/h)}^{-3}$, $M_* = -18.8$, $\alpha = -1.0$) with a hybrid selection function using the LFs from CfA2 North ($\phi_* = 0.05 \text{ (Mpc/h)}^{-3}$, $M_* = -18.67$, $\alpha = -1.03$) and CfA2 South ($\phi_* = 0.02 \text{ (Mpc/h)}^{-3}$, $M_* = -18.93$, $\alpha = -0.89$) as appropriate. The hybrid selection function results in insignificant changes to the model parameters:

$$\beta : -0.02 \pm 0.23 \rightarrow -0.05 \pm 0.26; \quad f_{\text{gal}} : 0.00_{-0}^{+0.24} \rightarrow 0.00_{-0}^{+0.25}. \quad (5-2)$$

Based upon Equations (5-1) and (5-2), we conclude that our density neighborhood technique is highly robust against uncertainty in the survey LF.

5.2. Choice of Smoothing Length

To determine the sensitivity of our results to the particular galaxy smoothing length, we repeat the analysis of §4 with smoothing kernels of $2.5h^{-1}$ Mpc and $10h^{-1}$ Mpc. These values are near the functional limits on kernel size: broader kernels wash out the large-scale structure we are hoping to probe, and narrower kernels are subject to excessive shot noise.

Figures 8 and 9, respectively, show the β and f_{gal} likelihood curves for kernel smoothing lengths of $2.5h^{-1}$ Mpc (dashed), $5h^{-1}$ Mpc (solid), and $10h^{-1}$ Mpc (dotted). As might be expected, the low-contrast $10h^{-1}$ Mpc smoothing length results in poorer parameter constraints; the high contrast of the $2.5h^{-1}$ Mpc smoothing gives tighter constraints. These curves do not include shot noise corrections (§5.3), which have a larger broadening effect at the smaller smoothing length. We give the 1σ confidence intervals on β and f_{gal} for the three smoothing lengths in Table 3. For the range of smoothing length $2.5\text{--}10h^{-1}$ Mpc, the maximum likelihood values for β and f_{gal} remain consistent with 0 (randomly distributed absorbers) at the 1.2σ level or less. Likewise, this range of smoothing lengths remains inconsistent with $\beta = 1$ (absorbers tracing structure) at the 3.8σ level or more. Thus our results are largely insensitive to the particular choice of smoothing kernel scale over a reasonable range.

5.3. Shot Noise in the Density Estimator

As a first estimate of the (n/\bar{n}) shot noise, we construct a mock redshift survey drawn from the CfA2 LF. We place the mock survey galaxies at random locations in redshift space, with the underlying density $(n/\bar{n}) \equiv 1$ throughout. We then remove galaxies fainter than the CfA2 magnitude limit and use the remaining

sample to estimate the density contrast throughout the survey volume. By construction, the (n/\bar{n}) shot noise throughout this homogeneous survey should only be a function of redshift. Figure 10 shows the variance of the density estimate, binned in $2.5h^{-1}$ Mpc radial intervals out to $150h^{-1}$ Mpc. Shot noise rapidly dominates the density estimate for $cz \gtrsim 12000 \text{ km s}^{-1}$, where the galaxies on average are separated by more than twice the $5h^{-1}$ Mpc smoothing length. Thus we restrict our analysis to Ly α absorption systems with $cz \lesssim 10500 \text{ km s}^{-1}$. The systematic decline in the median estimated density at random locations with $cz \gtrsim 10000 \text{ km s}^{-1}$ has virtually no influence on our test population of random locations (§4.3.1), drawn from the $cz_{\text{max}} \lesssim 10500 \text{ km s}^{-1}$ radial intervals of Table 1.

Unlike our mock survey, CfA2 is not homogeneous. The true shot noise will be relatively larger in regions of low galaxy number density, and vice versa. We reproduce this structure-dependent shot noise by bootstrap resampling the entire redshift dataset. We recompute the likelihood β and f_{gal} curves (eqs. 4-1 and 4-3) for 1024 bootstrap realizations of the redshift dataset. The 1σ bounds expand to $-0.26 < \beta < 0.22$, and $0.00 < f_{\text{gal}} < 0.25$, as compared with the ranges in §4.3. This minor increase grows large if we attempt to include the next two nearest Ly α systems, which are in the 3C 273 foreground at $cz \approx 15000 \text{ km s}^{-1}$. The large uncertainty (± 1 dex) in the density estimate at 15000 km s^{-1} overwhelms any benefit to be gained from the larger sample size. In §5.4, we discuss the observational requirements to include the 3C 273 absorbers at $z \gtrsim 0.05$ in our analysis.

5.4. Improving the Parameter Constraints with a Larger Sample

With 18 Ly α absorbers, the distribution of surrounding galaxy density contrasts places interesting constraints upon the nature of the low-redshift Ly α forest. A larger sample of absorber local densities should further shrink the error bars on the parameter constraints. Furthermore, local Ly α absorber searches along additional LOS would improve the likelihood that the cumulative path-length probes a representative distribution of the galaxy number density within the survey.

We quantify the improved constraints with a Monte Carlo simulation involving 50 mock absorbers placed along random LOS with the same mean frequency as our current sample. We assign redshifts to the mock absorbers according to an *a priori* β - or f_{gal} -model. The density contrast analysis recovers the seed values β or f_{gal} with 1σ error bars of only ~ 0.10 . Were the nearby Ly α absorbers

truly distributed randomly, for example, a distribution of density contrasts for 50 absorbers should conclusively rule out a model with $\beta = 1$ at the 9σ level. Assuming a local absorber frequency of $\sim 1/2500 \text{ km s}^{-1}$ detectable with *HST*/STIS, a sample of 50 absorber densities would require roughly a dozen AGN lines of sight within surveyed regions.

The current limits to the sample size of local Ly α absorber densities are: (1) the small number of AGN sightlines with identified low-redshift absorbers and (2) the limited depth of the complete redshift surveys for density estimation. As an example of the latter, there are ten more 3C 273 absorbers, with $0.05 \lesssim z \lesssim 0.16$, whose local densities cannot be estimated from a $m_{Zw} \leq 15.5$ redshift survey. Including all the additional 3C 273 absorbers would increase the sample size to 28 and almost double the cumulative pathlength currently probed by the various LOS in this study. Below we make a rough estimate of the observational requirements for studying the large-scale density environment around these more distant absorbers in a manner consistent with our current sample. Our technique differs substantially from the approach suggested by Sarajedini, Green, & Jannuzi (1996) for the even more distant ($0.2 < z < 0.4$) absorbers detected with *HST*/FOS.

To determine the (n/\bar{n}) profile along the entire 3C 273 LOS without significant edge dampening or shot noise, we need to survey galaxies brighter than $\sim M_*$ out to ~ 2 smoothing lengths, or $10h^{-1}$ Mpc, from the LOS. At $z = 0.05$ this corresponds to $B \sim 16.5$ over ~ 50 square degrees, decreasing to $B \sim 19.5$ over ~ 5.6 square degrees at $z = 0.16$. For comparison, Morris et al. (1993) have already surveyed ~ 3.5 square degrees around 3C 273 to $B \sim 19$, and Grogin et al. (1998) have recently completed a $2^h \times 12^\circ$ redshift survey around 3C 273 to the Zwicky catalog limit ($m_{Zw} = 15.7$).

6. Conclusions

We develop a new diagnostic for exploring the relationship between Ly α absorption systems and the galaxy distribution: we compare the CDF of the smoothed galaxy number density at the absorber locations with the density CDF for test populations within the redshift survey. The underlying assumption is that if Ly α absorbers sample the large-scale structure revealed by redshift surveys, the distribution of smoothed galaxy number densities around absorber positions in redshift space should be consistent with densities around galaxies in the redshift survey.

The procedure for evaluating the smoothed density field is straightforward,

requiring only the galaxy positions and redshifts, the survey selection function, and a choice of smoothing kernel. Moreover, this technique may be easily generalized as long as the redshift survey dimensions are large compared to the smoothing kernel. For sensitivity to large-scale structure without excessive blurring of the survey density contrasts, we adopt a Gaussian smoothing kernel of width $5h^{-1}$ Mpc, which is approximately the galaxy-galaxy correlation length.

The density CDF of 18 Ly α absorbers within regions surveyed to $m_{Zw} = 15.5$ is inconsistent with the comparable CDF for CfA2 galaxies. The K-S probability that the two CDFs are drawn from the same underlying distribution never exceeds 2×10^{-4} for a variety of CfA2 sampling geometries and weighting schemes (§§4.1, 4.2). The low probability results from a much larger fraction of Ly α absorbers than galaxies in underdense regions of the redshift survey. By contrast, a CDF of densities at randomly selected locations in the survey represents the same underlying density distribution as the Ly α absorbers with a K-S probability of 20%.

We explore the likelihood that the nearby Ly α absorbers are: (1) a single population distributed as the galaxy density raised to some power-law β , or (2) a dual population of absorbers, with a fraction f_{gal} distributed like the galaxies ($\beta = 1$) and the remainder distributed uniformly with respect to the galaxies ($\beta = 0$). For the 18 absorbers in this study, the $\pm 1\sigma$ likelihood interval of β is -0.02 ± 0.26 . The error bars include the uncertainty in the density estimator from the survey sampling variance and the uncertain survey LF, both small contributions. The maximum likelihood value of f_{gal} is 0.0, with a 1σ upper limit of 0.26. This value is consistent with the $f_{\text{gal}} \sim 0.20$ found by Mo & Morris (1994) for the 3C 273 absorbers alone, but at odds with the $f_{\text{gal}} = 0.65 \pm 0.18$ found by Lanzetta et al. (1995) for a sample of *HST*/FOS absorbers at higher column density.

We conclude that the low redshift, low column density Ly α clouds in this sample are *not* tracing the nearby large-scale structure marked by typical luminous galaxies. The absorbers appear in a range of density environments similar to those around randomly chosen locations throughout the survey. Thus the $N_{\text{HI}} \lesssim 10^{14} \text{ cm}^{-2}$ clouds at $z < 0.035$ are apparently similar in their spatial distribution to the unclustered, low column density clouds seen at high z (Sargent et al. 1980). The sharp decline in absorber metallicity at $N_{\text{HI}} \lesssim 10^{14}$ recently reported by Lu et al. (1998) suggests that the absorbers found nearby with *HST*/GHRS may be a distinct population from the *HST*/FOS absorber sample, which Lanzetta et al. (1995) argue is associated ($f_{\text{gal}} \sim 0.65$) with $\sim 160h^{-1}$ kpc galactic halos.

Although our sample is large enough to reject $f_{\text{gal}} = 1$, it does not exclude the conservative lower limit, $f_{\text{gal}} = 0.35 \pm 0.10$, of Lanzetta et al. (1995). In order to reduce the β and f_{gal} error bars to ± 0.10 , the precision necessary to exclude the Lanzetta et al. lower limit, Monte Carlo simulations indicate that a sample of ~ 50 nearby absorbers is required. The additional ~ 10 sightlines needed for a 50-absorber sample would also increase the likelihood that the cumulative path-length intersects the full range of density environments in the nearby universe. With the progress of wide-field imaging and multi-object spectroscopy, redshift surveys around the *HST* Ly α absorber sightlines using 4m-class telescopes should soon enable the density environment analysis presented here to encompass many more Ly α absorbers out to $z \lesssim 0.4$. Investigation of absorber density CDFs for subsamples grouped by column density might then reveal a contrast in absorber spatial distribution akin to the metallicity falloff seen by Lu et al. (1998).

We thank Susan Tokarz, Emilio Falco, and Michael Kurtz for assistance with the CfA2 survey database, and Jan Kleya for useful discussions. This research is supported in part by the Smithsonian Institution.

Table 1: Targets of Local Ly α Absorption Searches

Target	R.A. (B1950)	Dec. (B1950)	Redshift ^a (km s ⁻¹)	Ly α Sensitivity ^a (km s ⁻¹)
Mrk 335	00 ^h 03 ^m 45 ^s .2	+19°55′29″	7901	1713–7901
I Zw 1	00 ^h 50 ^m 57 ^s .8	+12°25′20″	18490	1660–10660
Mrk 421	11 ^h 01 ^m 40 ^s .6	+38°28′43″	9001	1501–9001
3C 273	12 ^h 26 ^m 33 ^s .2	+02°19′43″	47347	0–10500 ^b
Mrk 501	16 ^h 52 ^m 11 ^s .7	+39°50′25″	10301	1709–10301

^aGalactocentric velocities.

^bAbsorbers detected to $z \sim 0.12$, but CfA2 too sparse for meaningful density estimation.

Table 2: Local Ly α Absorption Velocities and Equivalent Widths

Background Source	cz_{abs} (km s ⁻¹)	W_{λ} (mÅ)	Background Source	cz_{abs} (km s ⁻¹)	W_{λ} (mÅ)
Mrk 335	2183	170	3C 273	2060	240
	2503	73		6413	27
	4483	26		7737	32
	6493	140		8704	120
I Zw 1	1777	120	Mrk 501	9750	74
	3021	84		4869	154
	5290	84		6209	36
Mrk 421	3047	92		7739	48
3C 273	890	371			
	1460	414			

Note. — Velocities are galactocentric. 3C 273 data from Morris et al. (1991), Bahcall et al. (1991), and Weymann et al. (1995); remaining data from Shull, Stocke, & Penton (1996).

Table 3: Results for Various Smoothing Kernel Scales

Param.	Kernel Smoothing Length		
	2.5 Mpc	5 Mpc	10 Mpc
β	0.09 ± 0.13	-0.02 ± 0.23	-0.45 ± 0.38
f_{gal}	$0.06^{+0.20}_{-0.06}$	$0.00^{+0.24}_{-0.00}$	$0.00^{+0.24}_{-0.00}$

Note. — 1σ (68.3%) confidence intervals, without corrections for shot noise or LF uncertainty.

REFERENCES

- Bahcall, J. N., Jannuzi, B. T., Schneider, D. P., Hartig, G. F., Bohlin, R., & Junkkarinen, V. 1991, *ApJ*, 377, L5
- Bahcall, J. N., & Spitzer, L. 1969, *ApJ*, 156, L63
- Bahcall, J. N., et al. 1993, *ApJS*, 87, 1
- Bajtlik, S. 1993, in Shull, J. M., Thronson, H. A., eds., *The Environment and Evolution of Galaxies*. Kluwer, Dordrecht, p. 191
- Bothun, G. D., & Cornell, M. E. 1990, *AJ*, 99, 1004
- Da Costa, L. N., Geller, M. J., Pellegrini, P. S., Latham, D. W., Fairall, A. P., Marzke, R. O., Willmer, C. N. A., Huchra, J. P., Calderon, J. H., Ramella, M., & Kurtz, M. J. 1994, 424, L1
- Geller, M. J., & Huchra, J. P. 1989, *Science*, 246, 897
- Grogin, N. A., Geller, M. J., & Huchra, J. P. 1998, in preparation
- Hernquist, L., Katz, N., Weinberg, D. H., & Miralda-Escudé, J. 1996, *ApJ*, 457, L51
- Hoffman, G. L., Lu, N. Y., Salpeter, E. E., Farhat, B., Lamphier, C., & Roos, T. 1993, *AJ*, 106, 39
- Hoffman, G. L., Lewis, B. M., & Salpeter, E. E. 1995, *ApJ*, 441, 28
- Huchra, J. P. 1976, *AJ*, 81, 952
- Huchra, J. P., Geller, M. J., De Lapparent, V., & Corwin, H., G., Jr. 1990, *ApJS*, 72, 433
- Huchra, J. P., Geller, M. J., & Corwin, H., G., Jr. 1995, *ApJS*, 99, 391
- Huchra, J. P., Vogeley, M. S., & Geller, M. J. 1998, *ApJS*, submitted
- Ikeuchi, S. 1986, *Ap&SS*, 118, 509
- Ikeuchi, S., & Turner, E. L. 1991, *ApJ*, 381, L1
- Jing, Y. P., Mo, H. J., & Boerner, G. 1998, *ApJ*, 494, 1
- Lanzetta, K. M., Bowen, D. V., Tytler, D., & Webb, J. K. 1995, *ApJ*, 442, 538
- Lu, L., Sargent, W. L. W., Barlow, T. A., & Rauch, M. 1998, *astro-ph/9802189*
- Lynds, R. 1971, *ApJ*, 164, L73
- Maloney, P. 1993, *ApJ*, 414, 41
- Marzke, R. O., Huchra, J. P., & Geller, M. J. 1994, *ApJ*, 428, 43 (MHG94)

- Marzke, R. O., Geller, M. J., da Costa, L. N., & Huchra, J. P. 1995, *AJ*, 110, 477
- Marzke, R. O., Huchra, J. P., & Geller, M. J. 1996, *AJ*, 112, 1803
- Mo, H. J., & Morris, S. L. 1994, *MNRAS*, 269, 52
- Morris, S. L., Weymann, R. J., Savage, B. D., & Gilliland, R. L. 1991, *ApJ*, 377, L21
- Morris, S. L., Weymann, R. J., Dressler, A., McCarthy, P. J., Smith, B. A., Terrile, R. J., Giovanelli, R., & Irwin, M. 1993, *ApJ*, 419, 524
- Oort, J. H. 1981, *A&A*, 94, 359
- Peebles, P. J. E. 1993, *Principles of Physical Cosmology* (Princeton University Press, Princeton)
- Pence, W. 1976, *ApJ*, 203, 39
- Prochaska, J. X., & Wolfe, A. M. 1997, *ApJ*, 487, 73
- Rauch, M., Weymann, R. J., & Morris, S. L. 1996, *ApJ*, 458, 518
- Rees, M. J. 1986, *MNRAS*, 218, 25p
- Sarajedini, V. L., Green, R. F., & Jannuzi, B. T. 1996, *ApJ*, 457, 542
- Sargent, W. L. W., Young, P. J., Boksenberg, A., Tytler, D. 1980, *ApJS*, 42, 41
- Sargent, W. L. W., Boksenberg, A., Steidel, C. C. 1988, *ApJS*, 68, 539
- Schechter, P. 1976, *ApJ*, 203, 297
- Shull, J. M., Stocke, J. T., & Penton, S. 1996, *AJ*, 111, 72 (SSP96)
- Slezak, E., de Lapparent, V., & Bijaoui, A. 1993, *ApJ*, 409, 517
- Stark, A. A., Gammie, C. F., Wilson, R. W., Bally, J., Linke, R. A., Heiles, C., & Hurwitz, M. 1992, *ApJS*, 79, 77
- Stocke, J. T., Shull, J. M., & Penton, S. 1995, *ApJ*, 451, 24
- Takamiya, M., Kron, R. G., & Kron, G. E. 1995, *AJ*, 110, 1083
- Tytler, D. A. 1987, *ApJ*, 321, 69
- Vogeley, M. S., Park, C., Geller, M. J., Huchra, J. P., & Gott, J. R., III 1994, *ApJ*, 420, 525
- Weymann, R. J. 1993, in Shull, J. M., Thronson, H. A., eds., *The Environment and Evolution of Galaxies*. Kluwer, Dordrecht, p. 213
- Weymann, R., Rauch, M., Williams, R., Morris, S., & Heap, S. 1995, *ApJ*, 438, 650

Zombeck, M. 1990, *Handbook of Space Astronomy and Astrophysics*, 2nd ed., (New York: Cambridge University Press)

Zwicky, F., Herzog, E., Wild, P., Karpowicz, M., & Kowal, C. T. 1961-8, *Catalogue of Galaxies and Clusters of Galaxies* (Pasadena: California Institute of Technology)

Figure Captions

Fig. 1.— Redshift survey slice and density profile along 3C 273 line of sight. See §3.2 for description.

Fig. 2.— Redshift survey slice and density profile along Mrk 335 line of sight. See §3.2 for description.

Fig. 3.— Redshift survey slice and density profile along Mrk 421 line of sight. See §3.2 for description.

Fig. 4.— Redshift survey slice and density profile along Mrk 501 line of sight. See §3.2 for description.

Fig. 5.— Redshift survey slice and density profile along I Zw 1 line of sight. See §3.2 for description.

Fig. 6.— Cumulative distribution function of galaxy density contrast around 18 nearby Ly α absorbers (solid), and around all CfA2 galaxies. The CfA2 sample’s CDF is shown with (dotted curve) and without (dashed curve) selection-function weighting (cf. §4.1).

Fig. 7.— Cumulative distribution functions of galaxy density contrast for various samples probing sightlines through the CfA survey, including: 18 nearby Ly α absorber locations from five AGN sightlines (solid); CfA2 galaxies within $2.5h^{-1}$ Mpc of random sightlines, with (dotted) and without (short dash) selection-function weighting (cf. §4.2); and random redshifts from random sightlines, with the same mean redshift spacing as the Ly α sample (long dash).

Fig. 8.— Likelihood curves for models with Ly α absorbers distributed as a power law β of the galaxy density contrast (cf. §4.3.1). Results shown for galaxy smoothing lengths of $2.5h^{-1}$ Mpc (dotted), $5h^{-1}$ Mpc (solid), and $10h^{-1}$ Mpc (dashed).

Fig. 9.— Likelihood curves for models with Ly α absorbers distributed in two populations, with a fraction f_{gal} distributed as the CfA2 galaxies and the remainder distributed randomly (cf. §4.3.2). Results shown for galaxy smoothing lengths of $2.5h^{-1}$ Mpc (dotted), $5h^{-1}$ Mpc (solid), and $10h^{-1}$ Mpc (dashed).

Fig. 10.— Variance in the $5h^{-1}$ Mpc density contrast, (n/\bar{n}) , within a simulated CfA2 survey of uniform density throughout (dotted line). The median value

(crosses) and $\pm 1\sigma$ bounds are shown for the density contrast sampled at a large ($N > 1000$) number of random locations within successive $2.5h^{-1}$ Mpc radial shells at distance D . Because of the growing systematic and statistical errors in the density estimator at $cz \gtrsim 12000$ km s $^{-1}$, we limit our analysis to Ly α absorbers with $cz < 10500$ km s $^{-1}$.

FIGURE 1

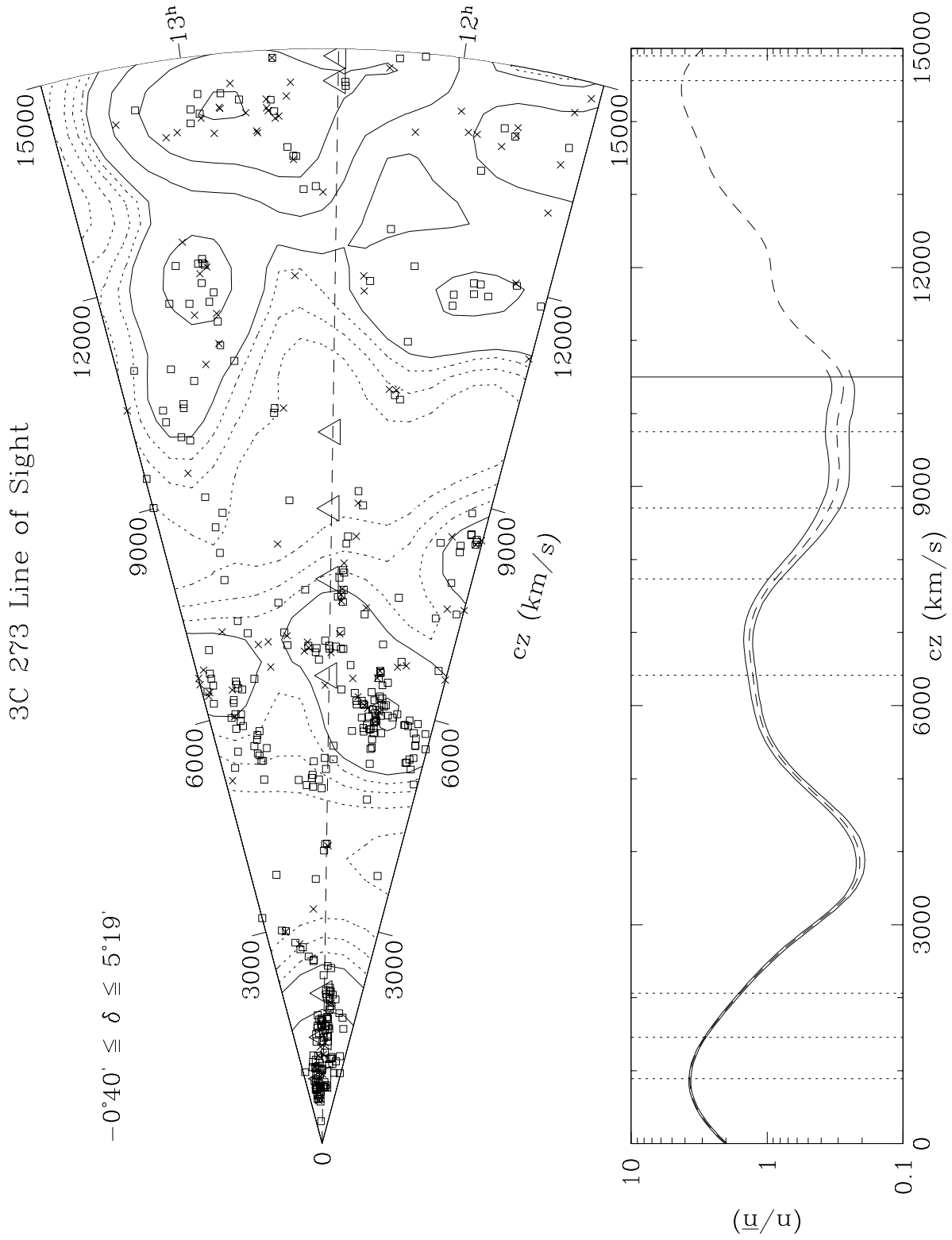


FIGURE 2

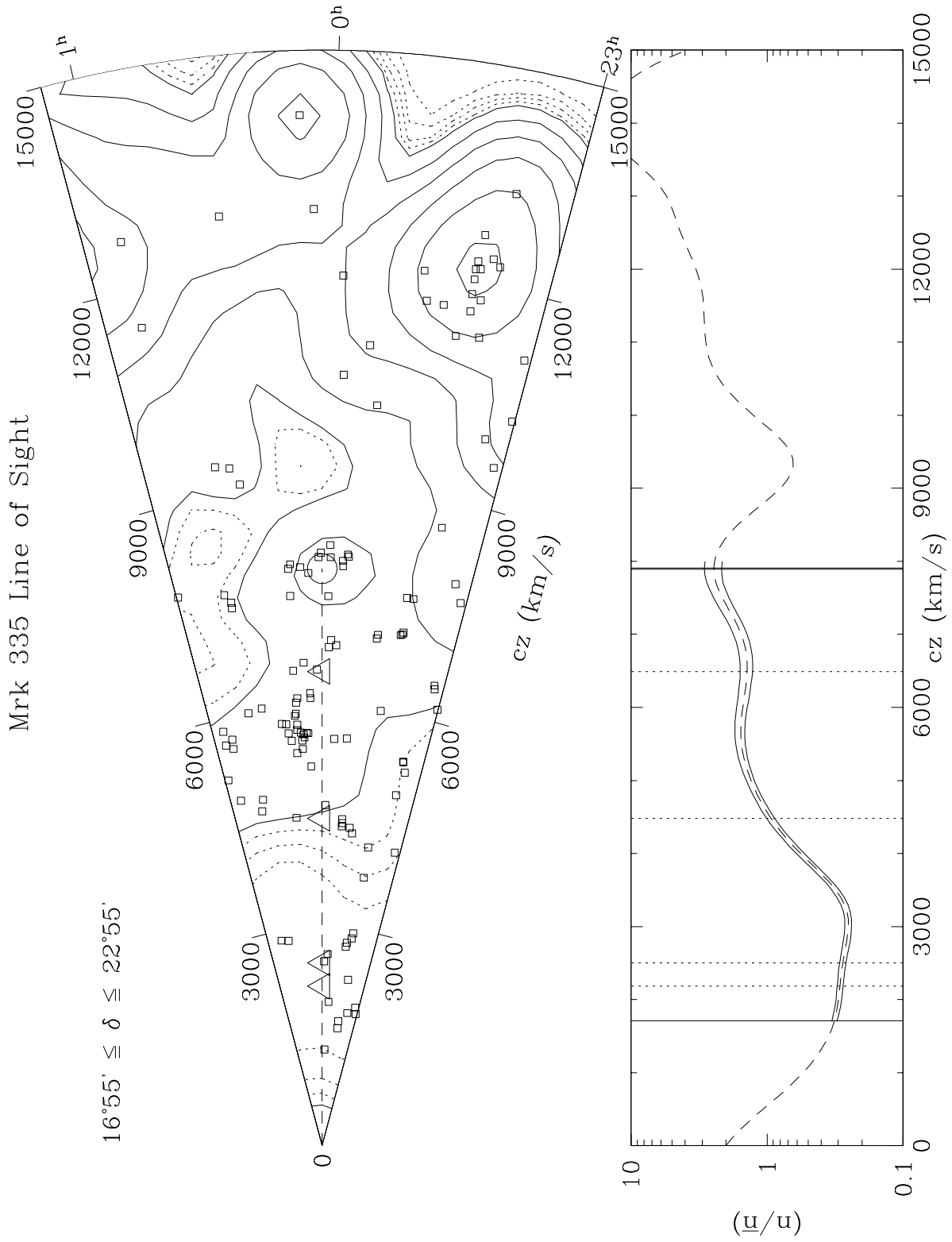


FIGURE 3

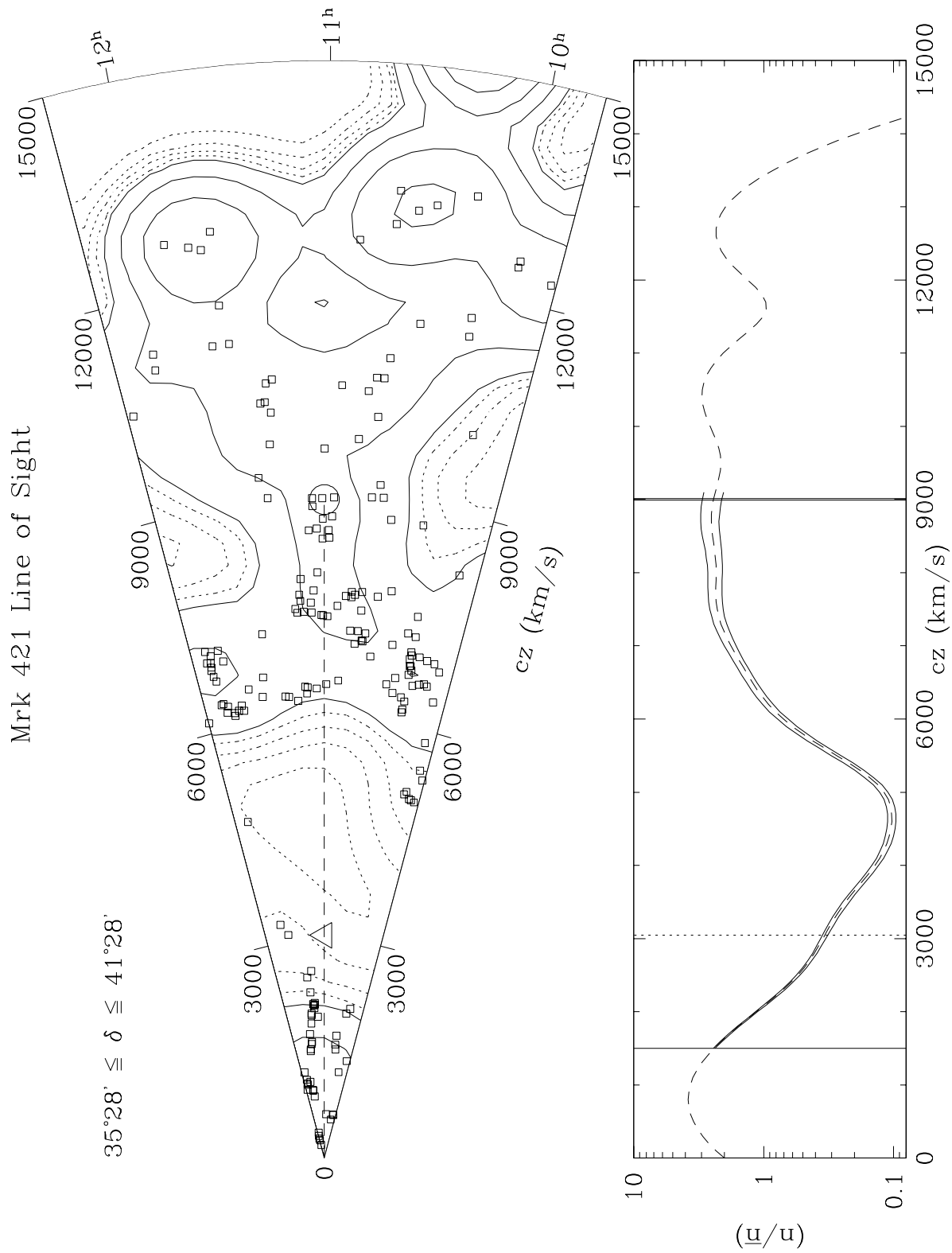


FIGURE 4

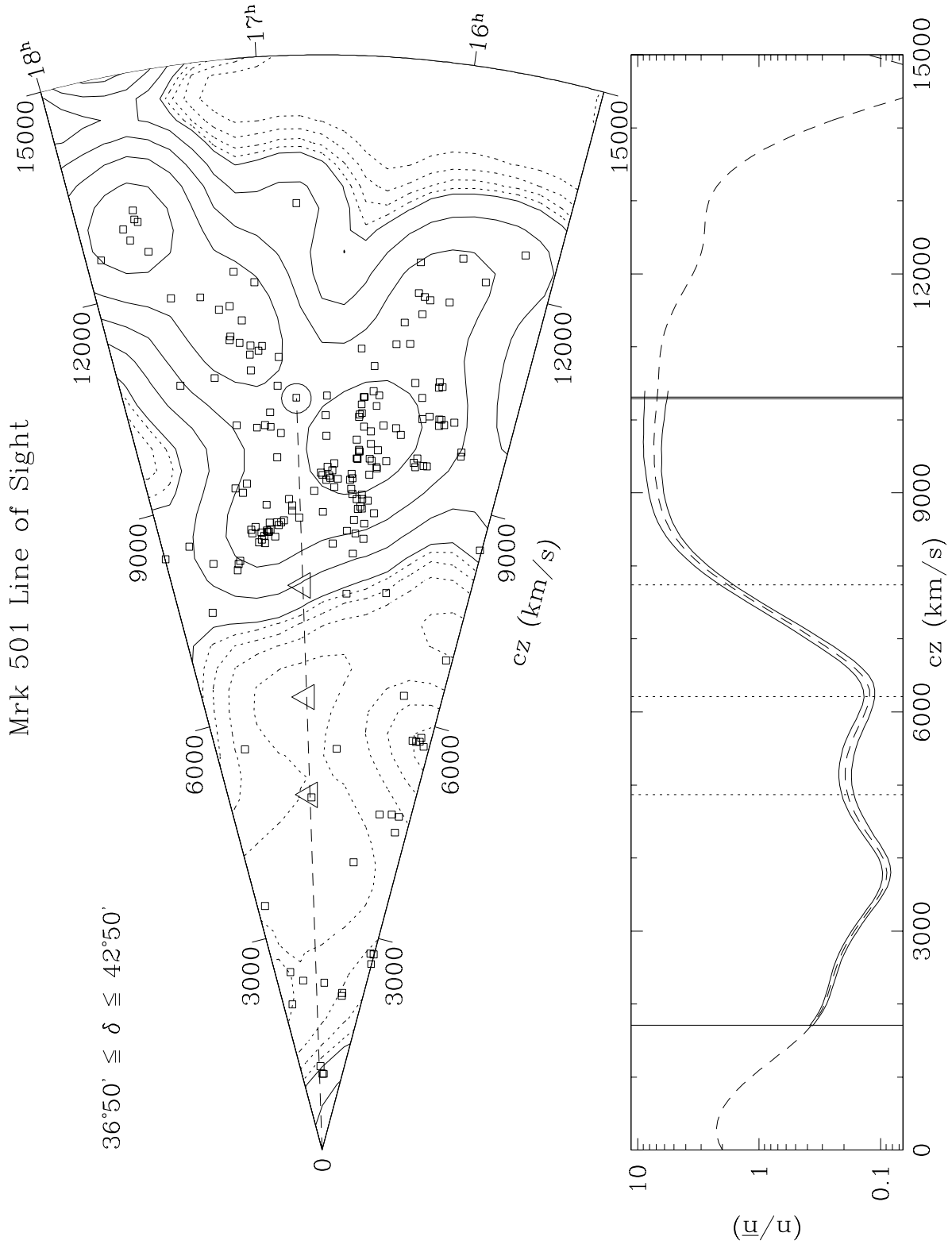


FIGURE 5

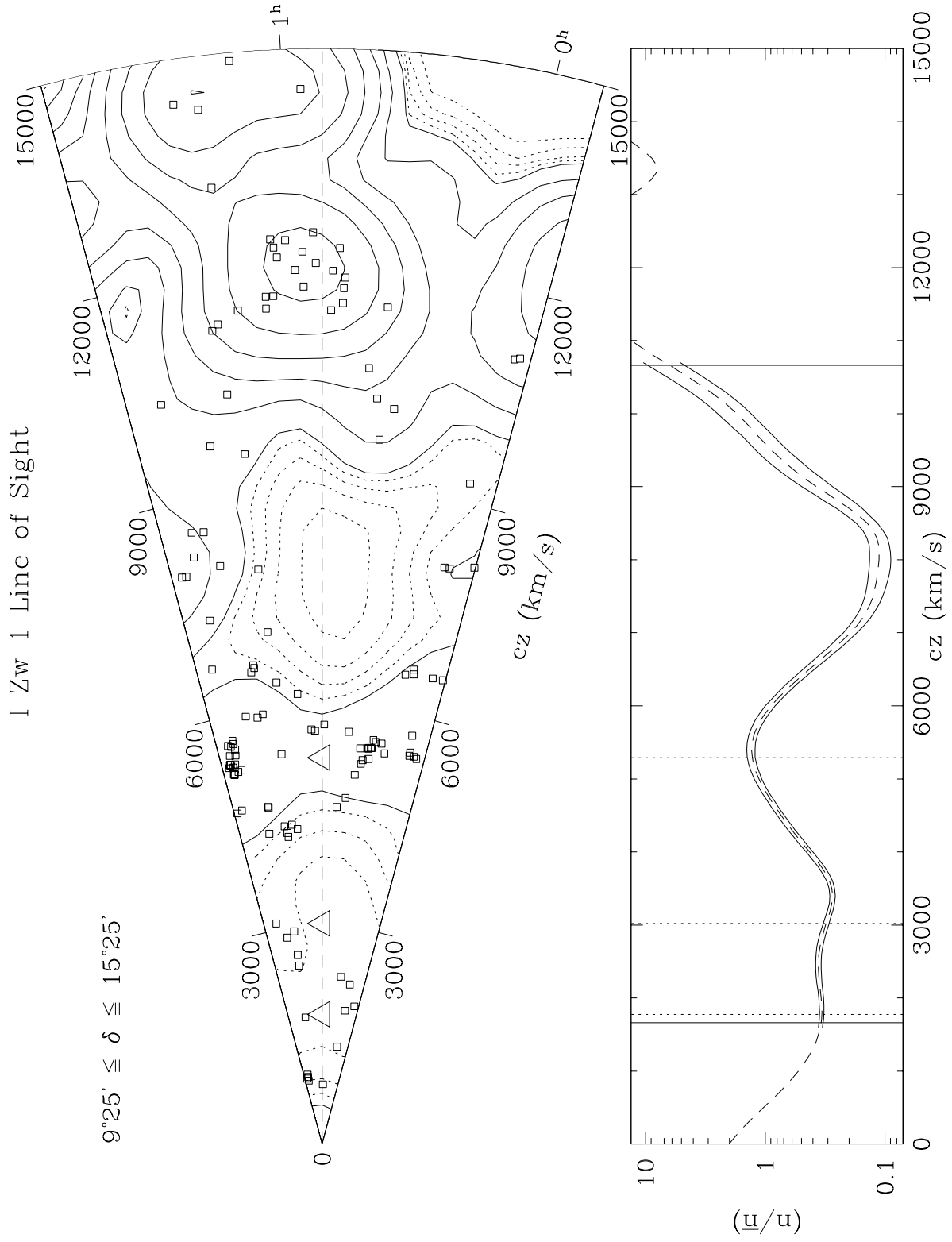


FIGURE 6

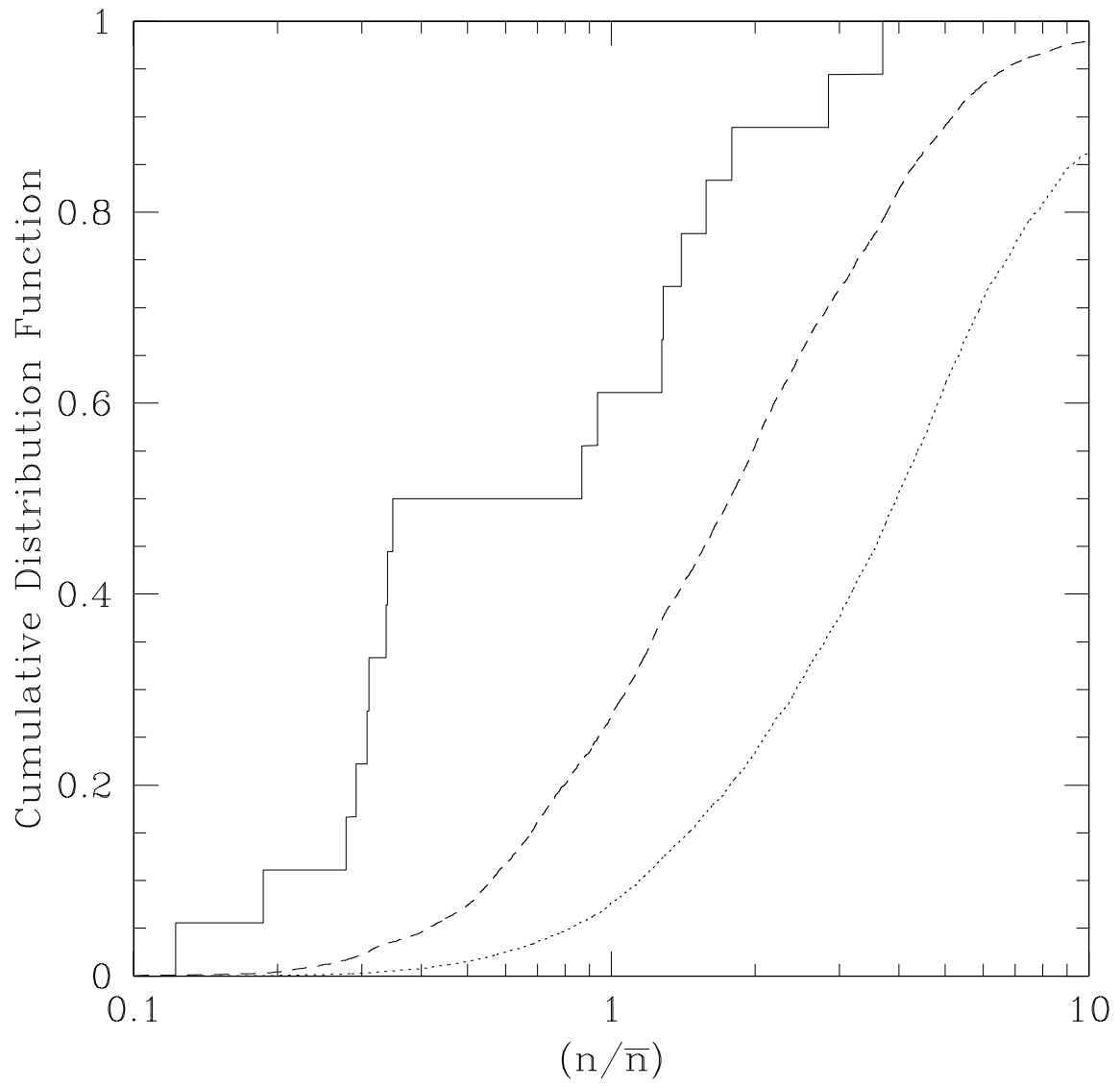


FIGURE 7

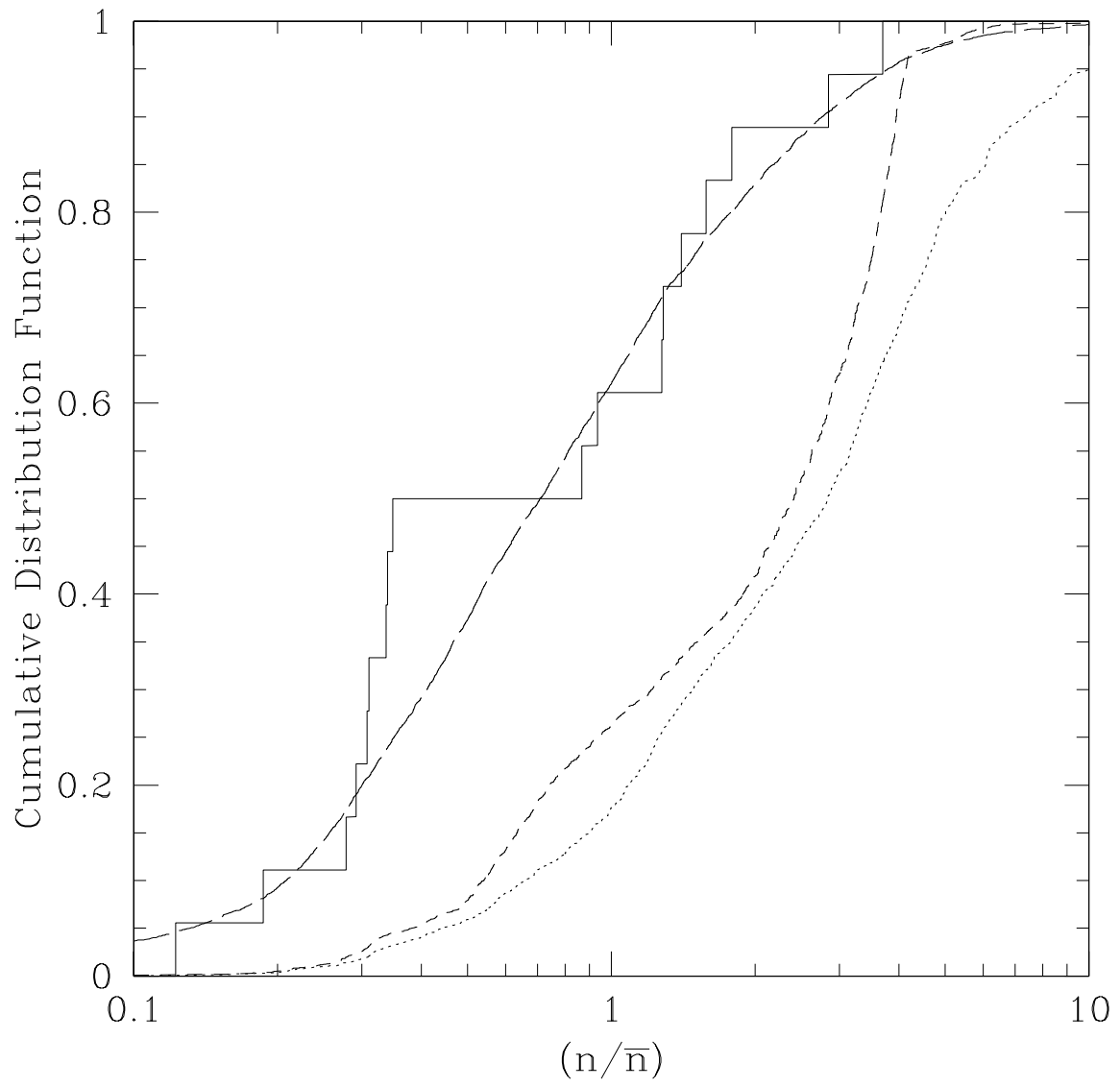


FIGURE 8

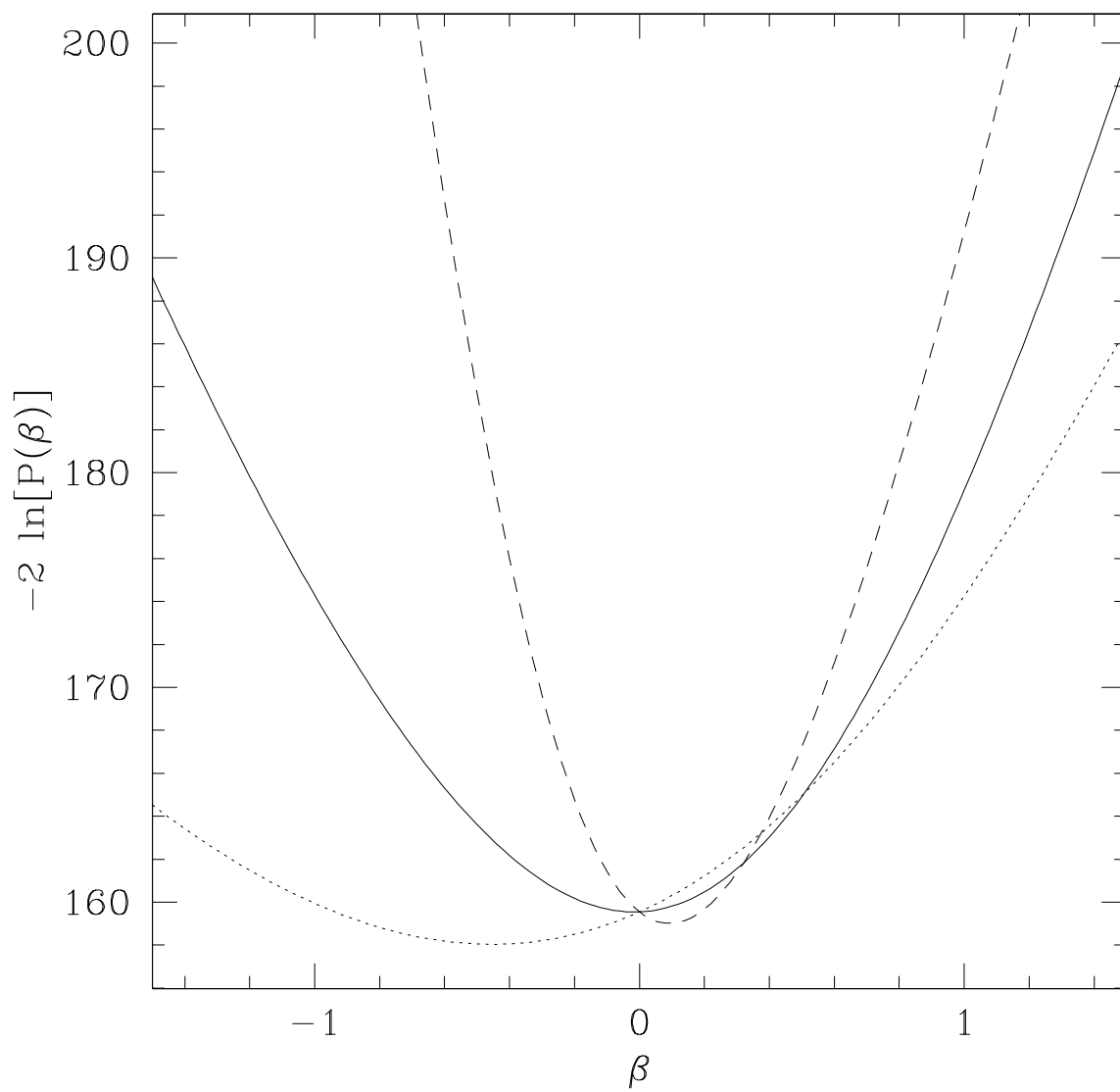


FIGURE 9

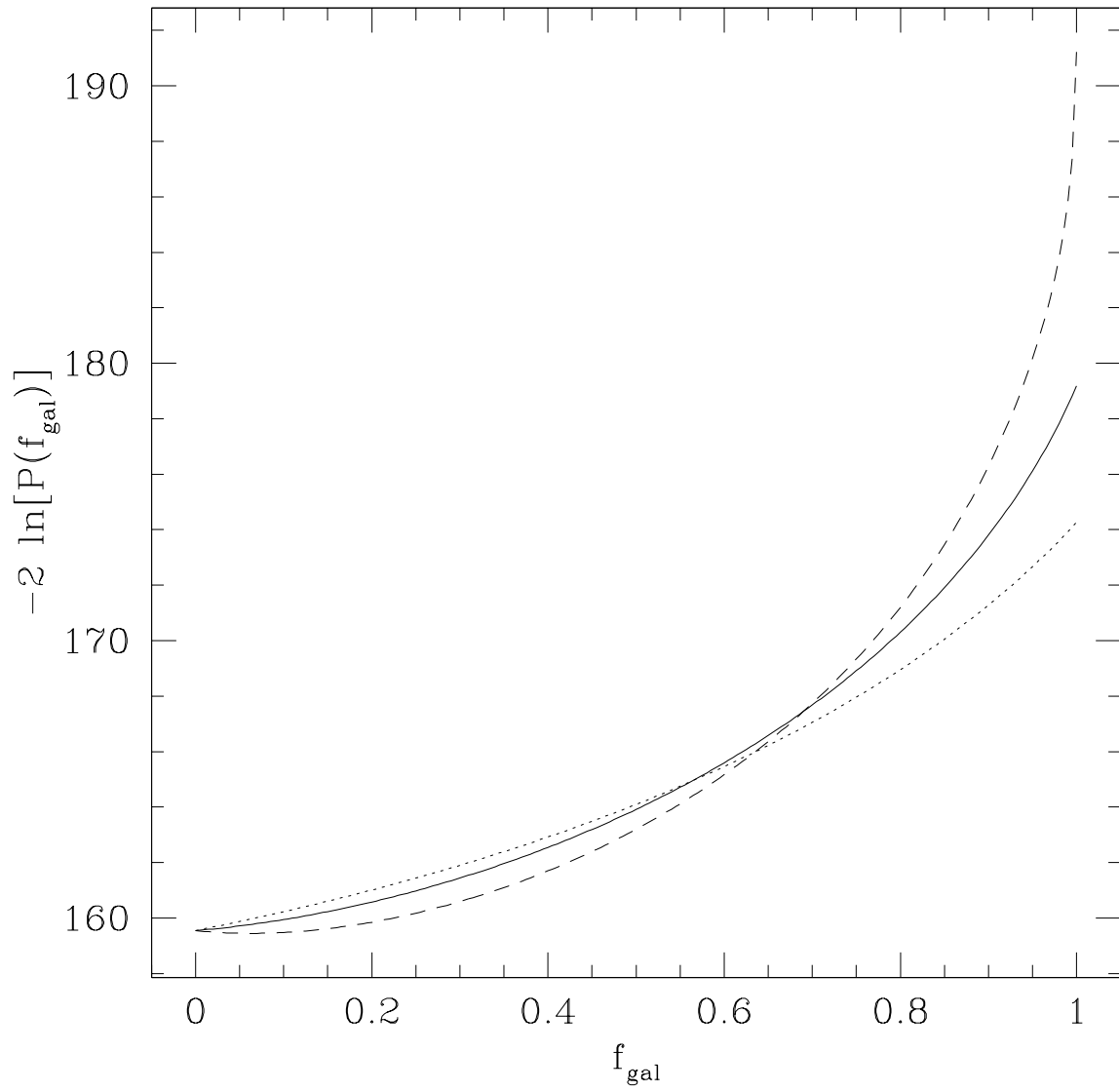


FIGURE 10

